doi:10.1016/j.jmb.2011.08.047 J. Mol. Biol. (2011) 413, 684–698

Contents lists available at www.sciencedirect.com

Journal of Molecular Biology

journal homepage: http://ees.elsevier.com.jmb

Iron-Coordinating Tyrosine Is a Key Determinant of NEAT Domain Heme Transfer

Jason C. Grigg, Cherry X. Mao and Michael E. P. Murphy*

Department of Microbiology and Immunology, Life Sciences Institute, The University of British Columbia, Vancouver, BC, Canada V6T 1Z3

Received 8 June 2011;
received in revised form
13 August 2011;
accepted 23 August 2011
Available online
26 August 2011

Edited by R. Huber

Keywords:
receptor;
Gram positive;
Staphylococcus aureus;
nutrient;
pathogenesis

In humans, heme iron is the most abundant iron source, and bacterial pathogens such as *Staphylococcus aureus* acquire it for growth. IsdB of *S. aureus* acquires Fe(III)–protoporphyrin IX (heme) from hemoglobin for transfer to IsdC via IsdA. These three cell-wall-anchored Isd (*i*ron-regulated *s*urface *d*eterminant) proteins contain conserved NEAT (*nea*r iron *t*ransport) domains. The purpose of this work was to delineate the mechanism of heme binding and transfer between the NEAT domains of IsdA, IsdB, and IsdC using a combination of structural and spectroscopic studies. X-ray crystal structures of IsdA NEAT domain (IsdA-N1) variants reveal that removing the native heme-iron ligand Tyr166 is compensated for by iron coordination by His83 on the distal side and that no single mutation of distal loop residues is sufficient to perturb the IsdA–heme complex. Also, alternate heme-iron coordination was observed in structures of IsdA-N1 bound to reduced Fe(II)–protoporphyrin IX and Co(III)–protoporphyrin IX. The IsdA-N1 structural data were correlated with heme transfer kinetics from the NEAT domains of IsdB and IsdC. We demonstrated that the NEAT domains transfer heme at rates comparable to full-length proteins. The second-order rate constant for heme transfer from IsdA-N1 was modestly affected (<2-fold) by the IsdA variants, excluding those at Tyr166. Substituting Tyr166 with Ala or Phe changed the reaction mechanism to one with two observable steps and decreased observed rates >15-fold (to 100-fold excess IsdC). We propose a heme transfer model wherein NEAT domain complexes pass heme iron directly from an iron-coordinating Tyr of the donor protein to the homologous Tyr residues of the acceptor protein.

Introduction

Iron is an integral component of many biological systems, where it is essential in catalysis and electron transfer for processes as fundamental as protein, DNA, and ATP syntheses.[1] Iron is typically limiting for microorganisms in their native environments, and many organisms have acquired systems to overcome iron restriction.[2,3] Free iron is especially limited in the human body, where it is found primarily in proteins such as ferritin, transferrin, and hemoglobin.[2] The most abundant iron source in

*Corresponding author. E-mail address: Michael.Murphy@ubc.ca.

Abbreviations used: heme, Fe(III)–protoporphyrin IX; IsdA-N1, IsdA NEAT domain; IsdB-N2, IsdB C-terminal-most NEAT domain; IsdC-N1, IsdC NEAT domain; IsdH-N3, IsdH C-terminal-most NEAT domain; PPIX, protoporphyrin IX; CoPPIX, Co(III)–protoporphyrin IX; PDB, Protein Data Bank; Fe(II)heme, Fe(II)–protoporphyrin IX; PEG, polyethylene glycol.

the human body is the Fe(III)–protoporphyrin IX (heme) molecule found in the O_2 carrier hemoglobin,[4] making it a prime target for specialized heme uptake systems to satisfy a pathogen's iron requirements.

Staphylococcus aureus is a successful pathogen and common cause of hospital-acquired infection.[5,6] Resistance to many antibiotics has spread throughout bacterial populations, and multidrug-resistant *S. aureus* strains are now commonly isolated from hospitals and are increasingly isolated from individuals with few predisposing risk factors within the community.[5,7] *S. aureus* possesses several iron acquisition systems that likely contribute to its ability to infect most tissues of the human body, including two siderophore biosynthetic loci,[8–10] siderophore transporters,[11–13] and more than one heme uptake system.[8,14,15]

Recently, there has been significant progress in the understanding of *S. aureus* ferric heme uptake through studies on the Isd (*i*ron-regulated *s*urface *d*eterminant) system.[14,16,17] The system is composed of at least nine proteins, including four cell-wall-anchored binding proteins: IsdA, IsdB, IsdC, and IsdH/HarA.[14,16] When hemoglobin is released by red blood cell lysis, it dissociates and oxidizes, forming methemoglobin. The oxidized Fe(III) form of heme is stripped from methemoglobin and transported across the bacterial cell wall,[18] followed by import through the membrane by means of an ABC transport system composed of IsdE, IsdF, and FhuC (substrate binding protein, permease, and a multifunctional ATPase, respectively).[19,20] Once in the cytoplasm, one of two heme-degrading enzymes (IsdG or IsdI) liberates the bound iron.[21–23]

In the *S. aureus* cell-wall-anchored Isd proteins, one to three copies of a NEAT (*nea*r iron *t*ransport) domain, consisting of ~125 amino acids, have been identified.[24] Spectroscopic studies demonstrated that heme iron is coordinated by a conserved Tyr residue in four of the *S. aureus* NEAT domains.[25–28] Structures of the IsdA NEAT domain (IsdA-N1),[29] the IsdB C-terminal-most NEAT domain (IsdB-N2),[30] the IsdC NEAT domain (IsdC-N1),[31] and the IsdH C-terminal-most NEAT domain (IsdH-N3)[32] have been determined in complex with heme.

Heme is bound by IsdA-N1 in a hydrophobic pocket with propionate groups at the molecular surface (Fig. 1a and b).[29] Heme iron is five-coordinate with a single-protein iron ligand, the Tyr166 phenolate, which in turn forms a H-bond with the Tyr170 phenol in an interaction thought to stabilize the Tyr166–iron ligand bond (Fig. 1b). Tyr170 is oriented to allow π-stacking interactions with a heme tetrapyrrole ring. Tyr166 and Tyr170 are both located in a β-strand on the proximal side of the heme pocket. Several hydrophobic residues line the base of the binding pocket, and a loop crosses the distal side of the heme (Fig. 1a). Three distal loop residues form H-bonds with the heme propionates: Lys75 and Ser82 form H-bonds with the more buried propionate group, and His83 forms a H-bond with the more solvent-exposed propionate (Fig. 1b).[29] Furthermore, the His83 imidazole ring is situated coplanar to the porphyrin ring ~3.4 Å from iron, thereby occluding access to the sixth

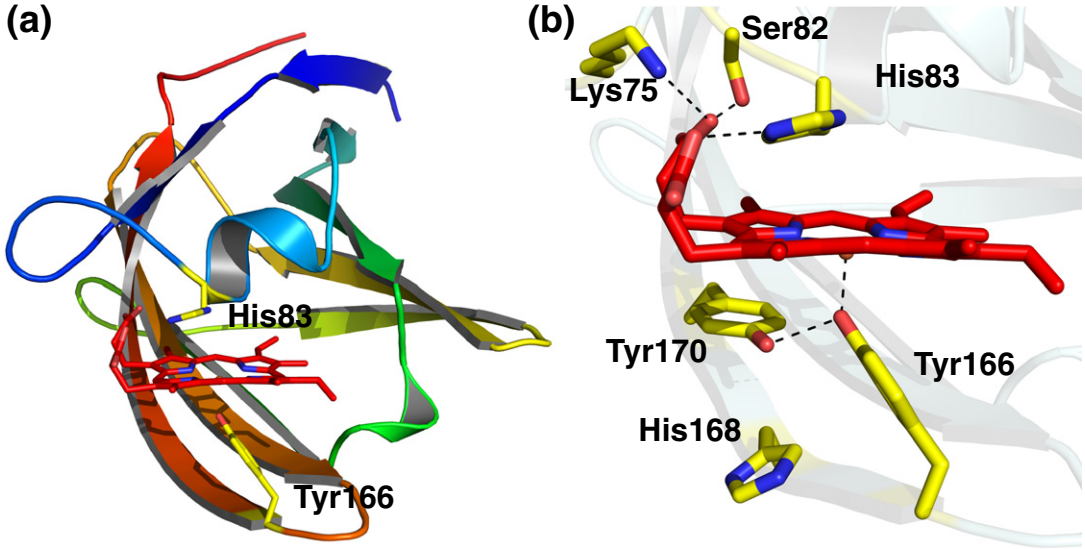

Fig. 1. Structure of IsdA-N1–heme. (a) Overall structure of the IsdA-N1–heme complex (PDB ID: 2ITF) shown as a cartoon colored from blue (N-terminus) to red (C-terminus). Heme and selected side chains are shown as sticks, with carbon shown in red and yellow, respectively. Oxygen, nitrogen, and iron are shown in red, blue, and orange, respectively. (b) Close-up of the wild-type binding pocket (PDB ID: 2ITF). Residues are shown as in (a). Hydrogen and metal ligand bonds are indicated by broken lines.

Table 1. Data collection and refinement statistics

	IsdA-N1 Y166A	IsdA-N1 H83A	IsdA-N1 K75A	IsdA-N1 + CoPPIX	IsdA-N1 wild type, reduced
Data collection[a]					
Resolution range (Å)	45–2.00 (2.07–2.00)	50–1.25 (1.32–1.25)	50–1.30 (1.35–1.30)	45–1.90 (1.93–1.90)	40–1.95 (2.02–1.95)
Space group	$P2_12_12_1$	$P2_1$	$P2_12_12$	$P2_1$	$P2_1$
Unit cell dimensions					
a, *b*, *c* (Å)	61.3, 96.8, 95.8	52.5, 51.8, 55.7	51.7, 76.6, 35.6	52.4, 51.8, 55.6	56.0, 58.6, 97.8
β (°)		91.9		91.7	93.0
Unique reflections	39,339	80,164	35,685	23,773	46,318
Completeness (%)	99.9 (99.9)	97.2 (87.0)	97.8 (83.7)	96.6 (78.1)	98.5 (87.9)
Redundancy	6.6 (6.4)	3.4 (2.5)	6.0 (3.1)	3.3 (2.5)	3.6 (2.8)
Average $I/\sigma I$	27.4 (4.7)	14.7 (5.3)	22.3 (3.0)	14.5 (3.1)	15.5 (2.4)
R_{merge}	0.07 (0.421)	0.046 (0.141)	0.06 (0.320)	0.091 (0.341)	0.08 (0.377)
Wilson *B*-factor (Å^2)	27.2	9.0	14.9	14.7	21.7
Refinement					
R_{work} (R_{free})	0.194 (0.235)	0.139 (0.164)	0.159 (0.185)	0.178 (0.223)	0.194 (0.244)
Number of water molecules	364	255	135	290	415
r.m.s.d. bond length (Å)	0.013	0.013	0.013	0.013	0.013
Average *B*-values (Å^2)	29.9	12.6	20.2	17.6	30.1
Ramachandran plot (%)					
Most favored regions	91.6	90.3	91.0	91.3	90.6
Disallowed regions	0.3	0.0	0.0	0.0	0.2
PDB ID	3QZN	3QZM	3QZL	3QZP	3QZO

[a] Data collection values in parentheses represent the data for the highest-resolution shell.

coordinate position. For the sake of clarity, all following discussions will refer to the Tyr166 face of the heme pocket as the proximal side and to the His83 side as the distal side, regardless of changes in heme-iron coordination.

The other *S. aureus* heme-binding NEAT domains bind heme in similar orientations with heme-iron coordination through a conserved proximal Tyr ligand. Recently, Zn^{2+}–protoporphyrin IX (PPIX) titration of IsdC-N1 was shown to cause ordering of the otherwise flexible loop located on the distal side of the porphyrin plane.[33] Other than a conserved Ser that forms a H-bond with a heme propionate, the residues of the putative flexible loop vary between NEAT domains.

The pathway of heme transport occurs from methemoglobin to IsdB or IsdH, then sequentially through IsdA and IsdC to the substrate binding protein IsdE for import through the permease.[18,34,35] These transfer reactions have been shown to occur between full-length recombinant Isd proteins and the NEAT domains alone. Here, we examine the mechanism of heme relay by following heme transfer both to and from variants of IsdA-N1. Several variants of residues involved in heme binding by IsdA-N1 were generated. From the results of a combination of X-ray crystallography and heme transfer assays, we propose a model for heme transport wherein NEAT domains pass heme directly from the heme-iron-coordinating Tyr of the donor protein to that of the acceptor protein. Analysis of protein–protein complex modeling and crystal packing offers further support for the proposed transfer model.

Results

We determined the crystal structures of the five forms of IsdA-N1, as follows: three variants (IsdA-N1 K75A, IsdA-N1 H83A, and IsdA-N1 Y166A), reduced wild-type IsdA-N1, and IsdA-N1 in complex with Co(III)–protoporphyrin IX (CoPPIX). All the structures were determined to 2.05 Å resolution or better and refined with good geometry (>90% of residues in the most favored regions and <0.5% of residues in the disallowed regions of a Ramachandran plot, as determined by PROCHECK).[36] Table 1 presents the crystallographic data collection and refinement statistics. Metalloporphyrin is bound in all five structures with minimal disorder, as shown by unambiguous electron density and average atomic *B*-factors of <30 Å^2. Furthermore, when compared to the wild-type heme-bound IsdA-N1 structure [Protein Data Bank (PDB) ID: 2ITF], none of these structures resulted in a significant alteration to the NEAT domain backbone conformation, with <0.5 Å r.m.s.d. for all main-chain atoms.[29] Notably, the r.m.s.d. variations observed were similar to those found when comparing the four molecules in the asymmetric unit of the wild-type IsdA-N1–heme structure.

Structures of IsdA-N1 variants

To gain insight into the potential roles of Lys75, His83, and Tyr166 in mediating heme binding and transfer by IsdA-N1, we produced the variants at these positions. Visible absorption spectra for the

heme-bound variants are shown in Fig. S1. Replacement of the heme-iron ligand Tyr166 with Ala results in heme-iron coordination by His83 on the distal side; the His83 imidazole ring is rotated ~90° about χ_2 such that $N^{\varepsilon 2}$ coordinates the iron atom (2.0 Å) (Fig. 2a and b). Heme is oriented in the pocket similarly to that in the heme-bound wild-type structure (Fig. 1a). However, the Y166A substitution removes the iron coordination potential of this residue on the proximal side of the heme, resulting in two distinct peptide conformers in the asymmetric unit. In chain A, a solvent molecule is bound in the sixth coordinate position of heme iron (Fig. 2a). Alternatively, in the other two molecules in the asymmetric unit, this solvent ligand is replaced by His168 $N^{\varepsilon 2}$ (2.1 Å) (Fig. 2b). The side chain of His168 is rotated into the binding pocket relative to chain A, causing a local disruption at residues 166 and 170 of the proximal β-strand. The pH dependence of the Y166A variant electronic state was examined by absorption spectroscopy to provide insight into heme coordination in solution (Fig. S2). At pH values below ~6.5, the absorption spectra resemble high-spin ferric heme (Soret band

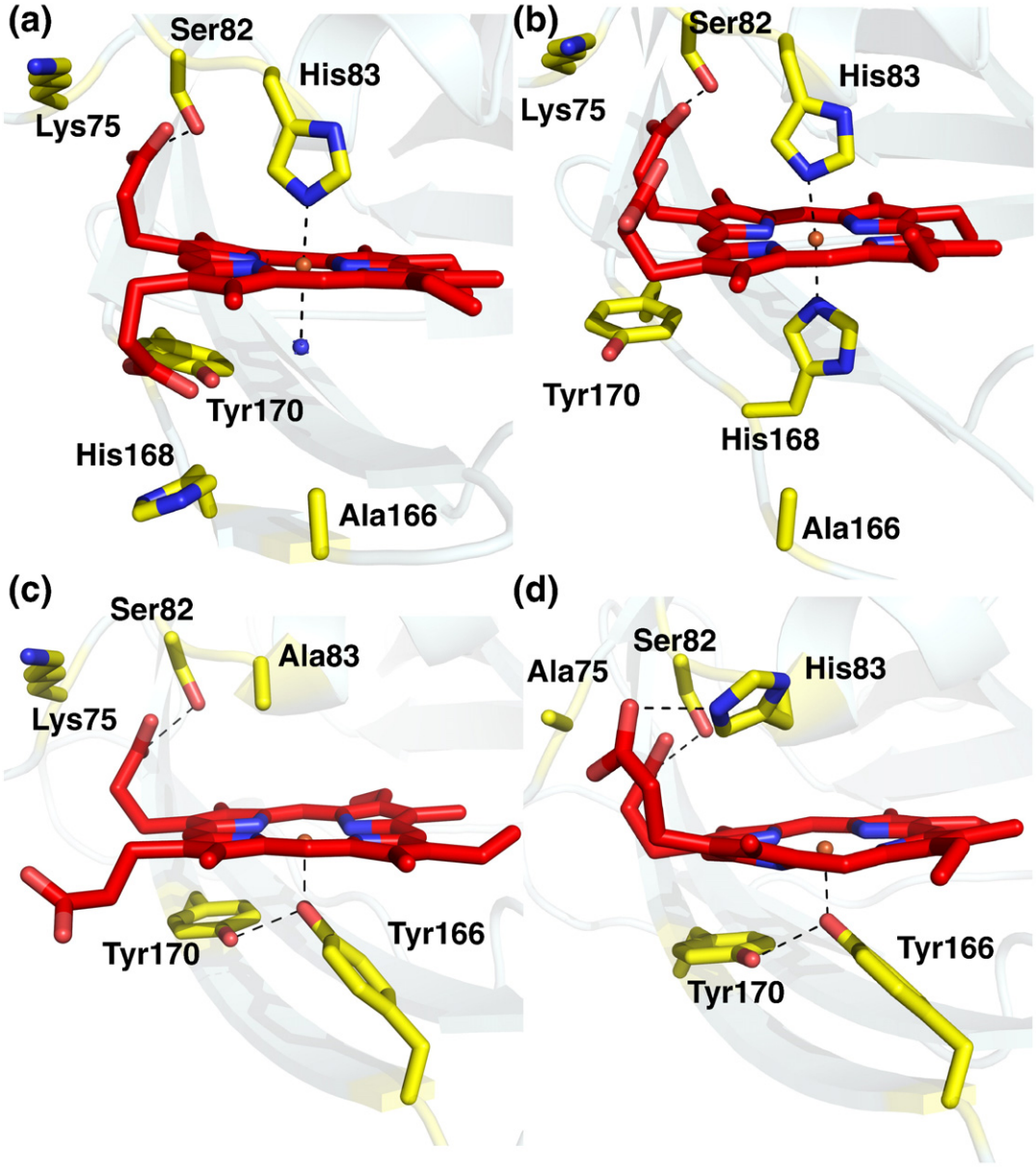

Fig. 2. IsdA-N1 variants. (a) Y166A chain A binding pocket. Atoms are colored as in Fig. 1b. The solvent molecule coordinated to heme iron is shown as a blue sphere. Hydrogen and metal ligand bonds are indicated by broken lines. (b) Y166A chain B binding pocket. (c) H83A binding pocket. (d) K75A binding pocket.

~403 nm; broad α/β band ~506 nm, 530 nm, and 635 nm); at pH values above 6.5, the spectra resemble low-spin ferric heme (Soret band ~412 nm; sharp α/β band ~530 nm and 560 nm). The transition from a state resembling high-spin iron to a state resembling low-spin iron suggests a switch from His–Fe–solvent to bis-His coordination, supporting the hypothesis that the two coordination spheres observed in the crystal structure are relevant in solution. The flexibility imparted by the Tyr-Ala replacement likely enables the observed alternate conformation of His168 in the heme-binding pocket of the crystal structure. For this reason, an IsdA-N1 Y166F variant was generated for an analysis of a more sterically similar replacement, although an X-ray crystal structure is not yet available.

Two residues that form H-bonds with the heme propionates and are in a loop that forms part of the distal side of the heme binding pocket were probed by the variants K75A and H83A. The crystal structure of the IsdA-N1 H83A variant reveals that the loss of the H-bond with the propionate results in an alternate conformation for this group (Fig. 2c). Nonetheless, the conformation of the distal loop is otherwise unchanged, likely due to interactions involving the remaining heme binding residues in the loop. Although the H83A substitution renders the sixth coordinate position of heme iron more solvent accessible, the position remains unoccupied and the heme iron is five-coordinate (Fig. 2c). In the wild-type structure, Lys75 forms a H-bond with the more buried propionate. However, in the K75A variant, the propionate remains well ordered, and the second H-bond with Ser82 is maintained (Fig. 2d). Additionally, the conformation of the residues that comprise the distal loop is unchanged. The weak effect of the K75A substitution on the IsdA-N1 fold is not surprising in retrospect, since sequence alignments reveal that position 75 is not conserved.[29]

Structures of IsdA-N1 in complex with Fe(II)–protoporphyrin IX and Co(III)PPIX

The contribution of ferric iron to heme binding was investigated by examining the structures of Co(III) and Fe(II)–protoporphyrin IX (Fe(II)heme) in complex with IsdA-N1. Replacement of Fe(III) by Co(III) results in a six-coordinate metal center with His83 (2.1 Å) and Tyr166 (2.4 Å) as ligands (Fig. 3a). The His83 imidazole rotates ~90° about χ_2 relative to the wild-type IsdA-N1–heme-bound structure such that $N^{\varepsilon 2}$ coordinates Co(III) (Fig. 3a). The pocket opens slightly to accommodate six-coordinate binding, highlighted by shifts away from the porphyrin ring (~0.9 Å by Tyr166 C^{α} and ~1.1 Å by His83 C^{α}) relative to the Fe(III)heme-bound IsdA-N1 structure. As in the IsdA-N1 H83A structure, the more exposed propionate group loses its lone protein H-bond and primarily adopts an altered conformation. The remainder of the CoPPIX environment is similar to that of the heme-bound structure.

The IsdA-N1–Fe(II)heme crystal structure was determined by growing IsdA-N1–heme crystals as previously described[29] and by reducing the central iron by soaking the crystal in cryoprotectant supplemented with 10 mM dithionite for ~10 min prior to immersion in liquid nitrogen. The crystals undergo an obvious color change in IsdA–heme from typical red brown to bright pink red, suggesting that heme reduction has taken place. In the

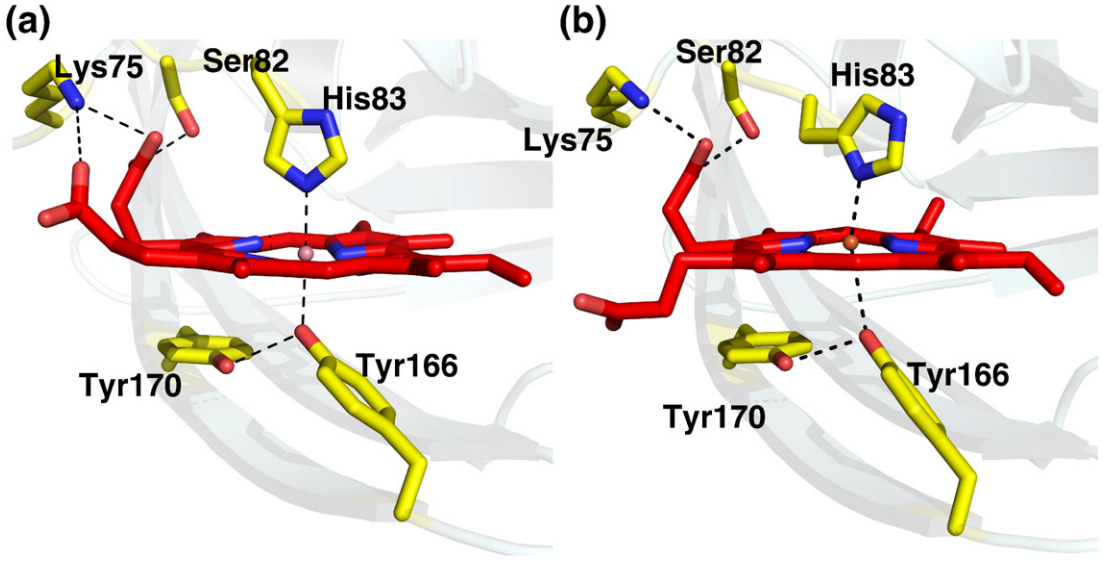

Fig. 3. The structures of IsdA-N1 bound to PPIX with altered metal centers. (a) The IsdA-N1–CoPPIX crystal structure. Atoms are colored as in Fig. 1b. Co(III) is shown as a purple sphere. (b) Reduced (Fe(II)heme) wild-type structure.

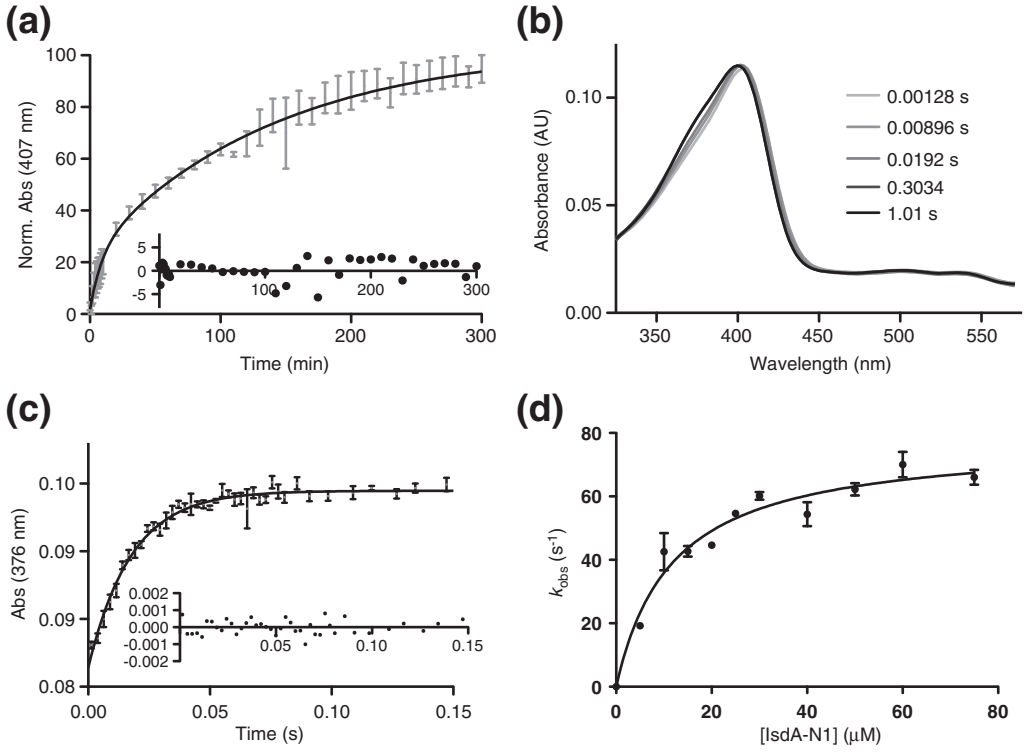

Fig. 4. IsdA-N1–heme binding and transfer. (a) Absorbance change over time in a mixture of 2 μM wild-type holo-IsdA-N1 and 50 μM apomyoglobin. Experiments were performed in duplicate. Data are shown as mean and standard error. The black curve is a two-phase exponential fit of the data. Inset: The residual plot. (b) Sample spectra for the transfer from 2 μM holo-IsdB-N2 to 20 μM apo-IsdA-N1. Maximal spectral change occurs at ~376 nm. (c) Data from (b) plotted as a change in absorbance at 376 nm to determine the observed transfer rate. A single-exponential fit to the data is shown in black. Inset: The residual plot of the fit. (d) The dependence of k_{obs} on the concentration of IsdA-N1 suggests a two-step transfer mechanism. The mean and standard error from five replicates are shown as black bars.

crystal structure, the central Fe(II) is five-coordinate by His83 $N^{\delta1}$ (2.2 Å) from the distal side (Fig. 3b). The His83 imidazole ring is rotated ~90° about χ_2, bringing it from parallel with the tetrapyrrole plane to perpendicular with the tetrapyrrole plane. However, in contrast to Fe(III) and Co(III) coordination in the IsdA-N1 Y166A and IsdA-N1–CoPPIX structures, respectively, the 90° rotation about χ_2 occurs in the opposite direction such that $N^{\delta1}$ coordinates Fe(II) rather than $N^{\varepsilon2}$. Rotation of the His83 side chain disrupts the H-bond between His83 $N^{\varepsilon2}$ and the more exposed heme propionate in the native structure, resulting in an altered propionate conformation with elevated *B*-factors. On the distal side of the heme pocket, structure superposition with IsdA-N1–heme reveals that the Fe(II)heme tetrapyrrole ring is positionally conserved in the pocket; nonetheless, the Tyr166 O^{η}–Fe(II) distance is stretched to ~3.0 Å. Otherwise, the same heme contacts are maintained in the Fe(II)heme-bound structure in chain A. Of the four molecules in the asymmetric unit, chains A and B undergo a shift from Y166 to H83 heme iron coordination as described above, whereas chains C and D more closely resemble the Fe(III)heme structure. However, chains C and D form a direct crystal contact involving atoms of the heme groups that likely hinders the conformational changes associated with the reduction from Fe(III) to Fe(II). The involvement of crystal contacts is consistent with the observation that crystals soaked in dithionite for more than 10 min began to crack and disintegrate.

Heme transfer to myoglobin

For each of the IsdA-N1 variants constructed, the rate of heme transfer to apomyoglobin was determined as an estimate of the heme off-rate. The use of apomyoglobin as a heme chelator is a well-established method for measuring off-rates.[37] Since previous work has demonstrated that IsdA does not directly interact with myoglobin[38] and that the rates are first order with respect to IsdA-N1 and independent of the apomyoglobin concentration (data not shown), the observed rate (k_{obs}) of spectral change is assumed to be a direct measure of the IsdA-N1–heme off-rate. The concentrations of the native and variant IsdA-N1–heme complexes were

determined by assaying heme concentration using the pyridine hemochrome assay.[39] Liu *et al.* determined a single off-rate from full-length IsdA to be 0.95 h^{-1}, whereas the transfer from the IsdA-N1 construct used in our studies is better described by a double-exponential equation (Fig. 4a).[34] The fast (k_{-1A}) and slow (k_{-1B}) off-rates are 2.6 h^{-1} and 0.42 h^{-1} (Table 2). Despite the presence of two observable rates compared to one observable rate for the full-length protein,[34] the overall rates are similar, supporting the hypothesis that the NEAT domain is the lone functional heme-binding region in IsdA.[25,27] Off-rates from all variants are also slow and were monitored for >3.5 half-lives (from 2 h to 15 h, depending on the variant). For all of the variants, the rates of absorbance change at 408 nm were best described by a double-exponential equation, excluding the H83A variant that was described well by a single exponential (Fig. 4a, Table 2; Fig. S3). Relative to the off-rate for wild-type IsdA-N1, the S82A variant releases heme with similar rates, the H83A and Y170F variants have ~3-fold decreased rates of heme release, and the Y166A and Y166F variants have 3-fold to 7-fold increased off-rates.

IsdB-N2-to-IsdA-N1 heme transfer

Tyr166 is the heme-iron ligand in IsdA and is therefore likely to participate in the heme transfer mechanism. Rates of heme reception from the heme-binding NEAT domain of IsdB (IsdB-N2) were monitored by stopped-flow spectroscopy for wild-type IsdA-N1 and Tyr166 variants. The heme transfer rate from IsdB-N2 (2 μM) to apo-IsdA-N1 (20 μM) was first determined as a baseline for comparison to variants. The maximal change in absorbance occurred at ~376 nm, and the rate of absorbance change at these concentrations was best described by a single exponential with an observed rate (k_{obs}) of ~57 s^{-1} (Fig. 4b and c). The k_{obs} for transfer between these NEAT domains is similar to the previously determined k_{obs} of ~115 s^{-1} for heme transfer from full-length holo-IsdB (3 μM) to full-length apo-IsdA (30 μM).[18] The correspondence in the rates implies that the NEAT domains alone are sufficient for rapid heme transfer between IsdB and IsdA and thus provide a model for transfer between full-length proteins. The concentration dependence of the IsdB-N2-to-IsdA-N1 heme transfer rates was determined for IsdA-N1 in 5-fold to 50-fold molar excess (Fig. 4d). The wild-type data fit a two-step model for heme transfer, similar to that previously described (Fig. 5).[30,34] In the model, the rate of complexation (k_1) is rapid relative to the rate of heme transfer (k_2) and assumes a rapid dissociation of the complex (k_3). Based on this model, values of 77 ± 3 s^{-1} and 11 ± 2 μM were computed for the rate of heme transfer (k_2) and the protein–protein dissociation constant (K_d), respectively.

Based on single-wavelength absorbance change, the Y166A and Y166F IsdA-N1 variants appear to have significantly diminished rates of transfer. The k_{obs} for transfer between 2 μM IsdB-N2 and 20 μM IsdA-N1 Y166A and Y166F is 0.44 s^{-1} and 1.7 s^{-1}, respectively. However, the absorbance spectrum at equilibrium is intermediate to that of heme-bound IsdB-N2 and IsdA-N1 Y166A/F, which reveals that only a fraction of heme bound to IsdB-N2 was transferred to IsdA-N1 (Fig. 6a). Since heme transfer is incomplete in these variants, the reverse reaction complicates analysis, and the rate constant obtained cannot be used for quantitative comparison to wild type. Despite the lack of quantitative comparison, it is clear that Tyr166 is required for a complete and efficient transfer to IsdA-N1.

IsdA-N1-to-IsdC-N1 heme transfer rates

The visible spectrum from the combination of any holo-IsdA-N1 variant tested and >10-fold excess apo-IsdC-N1 was essentially identical with that of holo-IsdC-N1, suggesting that transfer is pseudo

Table 2. Heme transfer kinetics of IsdA-N1 variants

IsdA variant	Apomyoglobin		Apo-IsdC-N1		
	k_{-1A} ± SE (×10^{-4} s^{-1})[a] *k*s	k_{-1B} ± SE (×10^{-4} s^{-1})[a]	k_{obs} ± SE[b] (s^{-1})	k_1 ± SE (μM^{-1} s^{-1})	k_2 ± SE (s^{-1})
Wild type	7.2 ± 3.6 [4%] 1.10.2 [96%]	1.1 ± 0.2 [96%]	16 ± 1	1.9 ± 0.1	ND
K75A	ND[c]	ND[c]	26 ± 1	4.0 ± 0.3	ND
S82A	5.4 ± 2.7 [18%]	0.5 ± 0.1 [82%]	15 ± 2	1.3 ± 0.1	ND
H83A	0.33 ± 0.02	0.33 ± 0.02	10 ± 4	1.7 ± 0.4	ND
Y166A[c]	44 ± 17 [27%]	8.6 ± 0.8 [73%]	2.3 ± 0.1	ND[d]	7.3 ± 0.4
Y166F[c]	23 ± 4 [42%]	4.4 ± 0.5 [58%]	5.8 ± 0.2	ND[d]	7.9 ± 0.2
Y170F	2.2 ± 1.1 [10%]	0.17 ± 0.03 [90%]	48 ± 2	3.6 ± 0.2	ND

ND, not determined in the model.
[a] Values in square brackets represent the percentage of the fast and slow rates.
[b] Observed transfer rate from 0.5 μM IsdA-N1 to 10 μM IsdC-N1.
[c] Not determined due to the stability of the protein at room temperature over the time course.
[d] Data fitted optimally by a two-step mechanism, with the first-order rate constant determined.

$$\text{heme-NEAT}_D + \text{NEAT}_A \underset{k_{-1}}{\overset{k_1}{\rightleftharpoons}} \text{heme-NEAT}_D\text{-NEAT}_A \underset{k_{-2}}{\overset{k_2}{\rightleftharpoons}} \text{NEAT}_D\text{-NEAT}_A\text{-heme} \underset{k_{-3}}{\overset{k_3}{\rightleftharpoons}} \text{NEAT}_D + \text{NEAT}_A\text{-heme}$$

Fig. 5. Model for heme transfer between Isd NEAT domains. The NEAT domain heme donor ($NEAT_D$) forms a complex with the heme acceptor ($NEAT_A$). Heme is then transferred within the protein–protein complex prior to dissociation.

first order and can be considered essentially unidirectional under the conditions tested (Fig. 6b). Under these conditions, the roles of Lys75, Ser82, His83, Tyr166, and Tyr170 in heme transfer from IsdA to IsdC were determined by stopped-flow spectroscopy for wild-type IsdA-N1 and variants at these positions. The largest spectral change between holo-IsdA-N1 and holo-IsdC-N1 was observed at ~376 nm. Absorbance change and the k_{obs} for heme transfer between IsdA-N1 (0.5 μM) and IsdC-N1, with concentrations ranging from 5 μM to 50 μM, were recorded (Fig. 6c and d). The k_{obs} of heme transfer from wild-type IsdA-N1 (0.5 μM) to IsdC-N1 (10 μM) was ~16 s^{-1}, similar to that determined (~24 s^{-1}) for transfer between full-length IsdA (1.2 μM) and full-length IsdC (~12 μM),[34] suggesting that efficient transfer between IsdA and IsdC can occur directly between NEAT domains. The k_{obs} values for wild-type IsdA-N1 and all variants, excluding Tyr166A/F, vary linearly with the concentration of IsdC-N1 when present in 10-fold to 100-fold excess, revealing only one readily

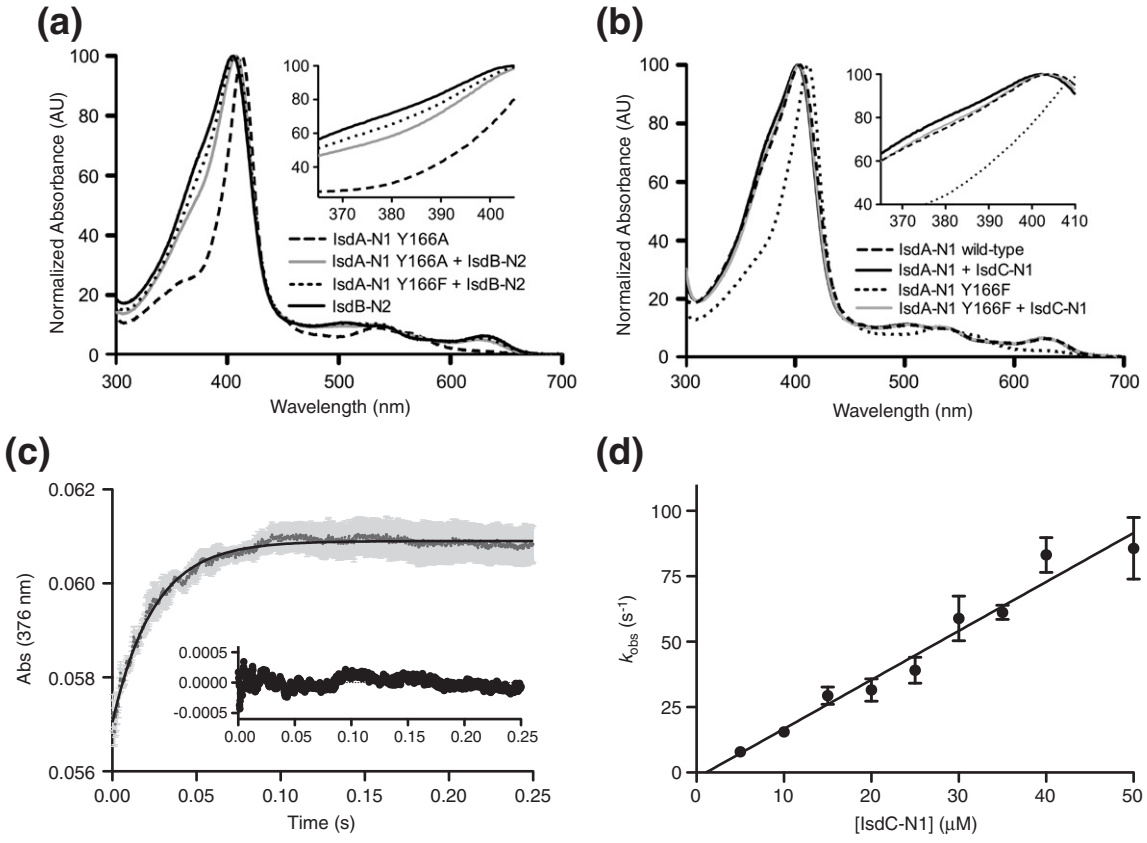

Fig. 6. Heme transfer into and out of IsdA-N1 variants. (a) Heme transfer from 2 μM holo-IsdB-N2 to 20 μM apo-IsdA-N1 Y166 variants. Heme is predominantly present in IsdB-N2 at equilibrium, as determined by spectra at equilibrium intermediate to the holo-IsdB-N2 and holo-IsdA-N1 Y166A/F spectra. Inset: A close-up of the region of the Soret band undergoing the largest absorption change. (b) Heme transfer from 2 μM holo-IsdA-N1 variants to 20 μM apo-IsdC-N1. The equilibrium spectra for the transfer from all IsdA-N1 variants to $IsdC_N$ overlay well, suggesting that heme exists primarily in IsdC-N1 at equilibrium. Inset: A close-up of the region of the Soret band undergoing the largest absorption change. (c) The change in absorbance over time of 0.5 μM wild-type holo-IsdA-N1 and 25 μM IsdC-N1. The black line is a single-exponential curve fit to the data, represented as the mean (dark gray) and error bars for the standard error of the mean (light gray). Inset: A plot of the residuals for the fit. (d) The k_{obs} concentration dependence for wild-type holo-IsdA-N1 to IsdC-N1 is linear over the concentrations tested, suggestive of a single observable step in the transfer reaction. Points are represented by the mean and standard error of five replicates. Data are summarized in Table 2.

observable kinetic step under the conditions tested (Fig. 6d; Fig. S4). The k_{obs} values for H83A were more variable than those for the other variants, as reflected in larger error estimates for k_1 (Table 2; Fig. S4d); however, despite the variability, a linear slope best described the data. From the previously proposed model for heme transfer (Fig. 5), the rate of protein–protein complexation (k_1) is likely rate limiting, with a relatively rapid rate of heme transfer (k_2). Most of the variants of the IsdA-N1–heme binding residues studied did not largely affect the second-order rate constant (maximal ~2-fold change relative to wild type) (Table 2). The k_{obs} for transfer from 0.5 μM IsdA-N1 Y166A (~2 s^{-1}) and Y166F (~6 s^{-1}) to 10 μM apo-IsdC-N1 is impaired by ~3-fold to 8-fold relative to wild-type rates. However, the concentration dependence of the transfer rates between the Y166A or Y166F IsdA-N1 variants and IsdC-N1 is best described by a transfer model with two observable steps (Table 2; Fig. S4), where values for k_2 and k_{-1}/k_1 are determined as previously described.[34] The value k_{-1}/k_1 is equivalent to the K_d of the transfer complex, and values of 11 μM and 2.3 μM were obtained for the complex of IsdC-N1 with IsdA-N1 Y166A and IsdA-N1 Y166Y, respectively. However, K_d values determined by these means have high error estimates. The change from a one-step mechanism to a two-step mechanism is attributed to a significantly impaired rate of heme transfer that is now rate limiting, rather than to domain complexation, under the conditions tested. Strikingly, these decreases in rates for IsdA-N1 Y166A/F heme transfer to IsdC-N1 relative to the other IsdA-N1 variants are observed despite increased off-rates for these Tyr166 variants to apomyoglobin.

Discussion

S. aureus uses the multicomponent Isd system to transport heme across the cell wall and cytoplasm to satisfy its iron requirement.[14] IsdA plays a central role in the cell wall by relaying heme from the surface receptors IsdB and IsdH to IsdC.[18,35] The C-terminal NEAT domains are the main functional heme binding unit in the cell-wall-anchored Isd proteins, as evident from heme-bound crystal structures and the kinetics of heme binding and transfer. For full-length IsdA, the rate of heme release (off-rate) from the NEAT domain is >1000-fold slower than the rates of heme transfer from IsdB or heme transfer to IsdC, supporting the hypothesis that an activated complex is formed and sufficient for heme transfer catalysis.[18,34] The IsdA-N1 NEAT domain recapitulates most of the heme transfer functions described previously for the full-length protein. Recently, we showed that heme transfer from IsdB-N2 to IsdA-N1 follows a two-step mechanism, with rates that are comparable to those observed for soluble full-length forms.[30] Heme transfer from full-length IsdA to IsdC also occurs with two observable steps, namely the association of a holo-IsdA–apo-IsdC complex followed by the transfer of heme to yield an apo-IsdA–holo-IsdC complex prior to dissociation.[34] In contrast, a one-step kinetic model better describes the IsdA-N1-to-IsdC-N1 transfer data, implying that protein–protein complexation is rate limiting for transfer between IsdA-N1 and IsdC-N1. The different kinetic model for heme transfer between full-length Isd proteins[34] relative to the NEAT domains could reflect differences in experimental conditions. Alternatively, these differences suggest that regions outside the NEAT domains could enhance protein–protein interactions. Work to identify additional functional regions outside the NEAT domains is ongoing. Nonetheless, the overall heme transfer rate for the NEAT domains is comparable to that for the full-length proteins and remains greatly enhanced over the off-rates.

To provide insight into the roles of specific residues in IsdA ligand binding and transfer to and from the IsdB NEAT domain and IsdC-N1, we produced and analyzed the heme binding pocket point variants by a combination of X-ray crystallography and stopped-flow spectroscopy. The IsdA-N1 distal loop (residues 75–87) makes several direct heme contacts. Lys75, Ser82, and His83 form H-bonds with the propionate groups; Met84 forms hydrophobic interactions; and a stacked π-bonding interaction is observed between Tyr87 and the most buried heme pyrrole ring. In the presence of heme, single-site substitutions from Lys75, Ser82, or His83 to Ala were not sufficient to disrupt the structure of the IsdA-N1 distal loop, suggesting that loop stability is a cumulative result of these interactions. Recently, NMR studies of IsdC-N1 demonstrated that porphyrin binding stabilizes an otherwise flexible distal loop.[33] In contrast, the apo-IsdA-N1 crystal structure closely resembles the holostructure other than the rotation of the side chain of His83 and a modest displacement of Met84 into the pocket.[29] Nonetheless, the IsdA-N1 binding pocket is sufficiently malleable to accommodate alternative metal coordination, such as that observed with CoPPIX and Fe(II)heme, by exploiting the availability of His83 and Tyr166 (Fig. 3a and b). Crystal contacts in the apo-IsdA-N1 structure may have stabilized the distal loop in the same conformation as the holo form, and the loop could undergo a similar disordered-to-ordered transition in solution, as seen in IsdC-N1. Since residues in the distal loop contact heme rather than the remainder of the protein,[29] the flexibility of the loop is likely a general feature of apo NEAT domains.

Residues that form the distal loop are variable in *S. aureus* heme-binding NEAT domains.[17] Ser82 is

the only distal loop residue that is absolutely conserved among these domains. His83 is replaced by Met, Ile, and Val in IsdB-N2, IsdC-N1, and IsdH-N3, respectively. The X-ray crystal structures of IsdA-N1 Y166A, IsdA-N1–Co(III)PPIX, and IsdA-N1–Fe(II)PPIX demonstrate that His83 can replace or augment Tyr166 as the metal ligand. Furthermore, the ability of His83 to coordinate ferrous heme is supported by spectroscopic data on full-length IsdA. Reduction of IsdA–heme resulted in spectra resembling high-spin five-coordinate ferrous heme with a single axial His ligand.[27] The Isd system would likely predominantly transport Fe(III)heme rather than Fe(II)heme, making the physiological utility of His83 in IsdA unclear; however, if Fe(II) heme is encountered, IsdA could function in its sequestration. Alternatively, His83 occludes access to the distal side of heme iron by potential small-molecule ligands[27] and thus could mediate access to the sixth coordinate position for transfer. Since histidine is a common iron ligand, it is tempting to speculate that His83 may have a role in heme transfer.

Within IsdA, Tyr166 and His83 are both situated such that either residue could receive heme iron from the donor or could pass heme iron. Transfer rates to and from IsdA-N1 variants were measured and compared to wild-type rates to determine what residues play a key role in receiving and donating heme. Equilibrium for heme transfer from all holo-IsdA-N1 variants to apo-IsdC-N1 is reached rapidly and essentially complete in IsdC-N1. Relative to wild-type IsdA-N1, the second-order transfer rates from the K75A, S82A, H83A, and Y170F variants are within ~2-fold of the wild-type rate. The IsdA-N1 H83A variant crystal structure reveals that the distal iron coordination site remains unoccupied in the absence of the His83 imidazole ring. Combined with the small change in observed transfer rate, the IsdA-N1 H83A structure suggests that His83 does not play a direct role in heme transfer from IsdA. The primary role of His83 in IsdA is likely to secure the more solvent-exposed heme propionate and potentially gate access to the distal heme-iron position.

Tyr166 variants were significantly impaired in heme transfer rates both to and from IsdA-N1 despite an increase in the off-rate (Fig. 6a, Table 2). For heme transfer from IsdB-N2 to IsdA-N1 Y166 variants, spectra suggest that, at equilibrium, heme is preferentially bound by IsdB-N2 even when the variant is present in >10-fold excess. Although a transfer rate could not be determined for these variants, Tyr166 is clearly essential for maintaining directional heme transfer from IsdB to IsdA. The IsdA-N1 Y166A crystal structure reveals that His83 serves as the heme-iron ligand on the distal side in this variant (Fig. 3b). Since His168 can also form an iron ligand blocking the proximal coordination site, a more sterically subtle Y166F variant was made, although transfer rates were comparable to Y166A (Table 2). The Y166A and Y166F substitutions change the heme transfer kinetic model from a second-order reaction, where k_{obs} varies linearly with the concentration of apo-IsdC-N1, to a first-order reaction, where k_{obs} values plateau at high apo-IsdC-N1 concentrations. The rate-limiting step in Y166A/F transfers is likely the rate of heme transfer (k_2) instead of the rate of complexation (k_1), as observed for the other variants (Fig. 5). As a result, the effect of the substitutions on heme transfer is accentuated at high apo-IsdC-N1 concentrations (e.g., rate impairment by >15-fold at 50 μM apo-IsdC-N1). In *S. aureus*, the Isd proteins are highly expressed within the cell wall upon iron restriction,[40] resulting in a high local concentration of NEAT domains. Therefore, the *in vivo* condition may be more accurately modeled *in vitro* at relatively high concentrations of apoacceptor, where proximal tyrosine coordination is essential. The impaired heme transfer rates both from holo-IsdB-N2 to apo-IsdA-N1 Y166A/F and from holo-IsdA-N1 Y166A/F to apo-IsdC-N1 suggest that tyrosinate–iron coordination or an open distal position is required for rapid heme transfer to IsdC-N1 or rapid heme transfer from IsdB-N2.

Together, the data suggest a model in which heme is transferred by forming an intermediate, with heme shuttling directly from the Tyr ligand of the donor protein to the Tyr ligand of the acceptor protein. This model is preceded by the model proposed for the single Met-Ala variants in Shp.[41] Two models have been developed for heme transfer from the *Streptococcus pyogenes* NEAT domain homolog Shp to the IsdE homolog SpHtsA.[41] In the first mechanism for heme transfer, an Shp–SpHtsA complex is formed, followed by heme-iron release from coordinating Met residues of Shp. Heme is transferred as an unstable intermediate preceding iron coordination by the His-Met pair from SpHtsA.[41] The second mechanism, supported by kinetic data on single Met-to-Ala substitutions at either coordinating Met in Shp, involves ligand exchange and a six-coordinate heme-iron intermediate. In the intermediate, the lone remaining Met from Shp and one of the SpHtsA ligands coordinate heme iron, followed by replacement of the Met ligand of Shp by the second SpHtsA ligand.[41]

A model for the Isd system, wherein heme is transferred from IsdB-N2 to IsdA-N1 by a direct access of Tyr166 to the distal site of the IsdB-N2 heme iron, was constructed. From IsdA-N1, heme iron is then directly passed to IsdC Tyr132, which again coordinates heme iron on the distal side of IsdA-N1 (Fig. 7). This transfer model is consistent with the ability of IsdA-N1 to bind heme in both orientations related by 180° about the heme α,γ-meso axis, which would allow heme to enter in either of the two orientations, as required for direct

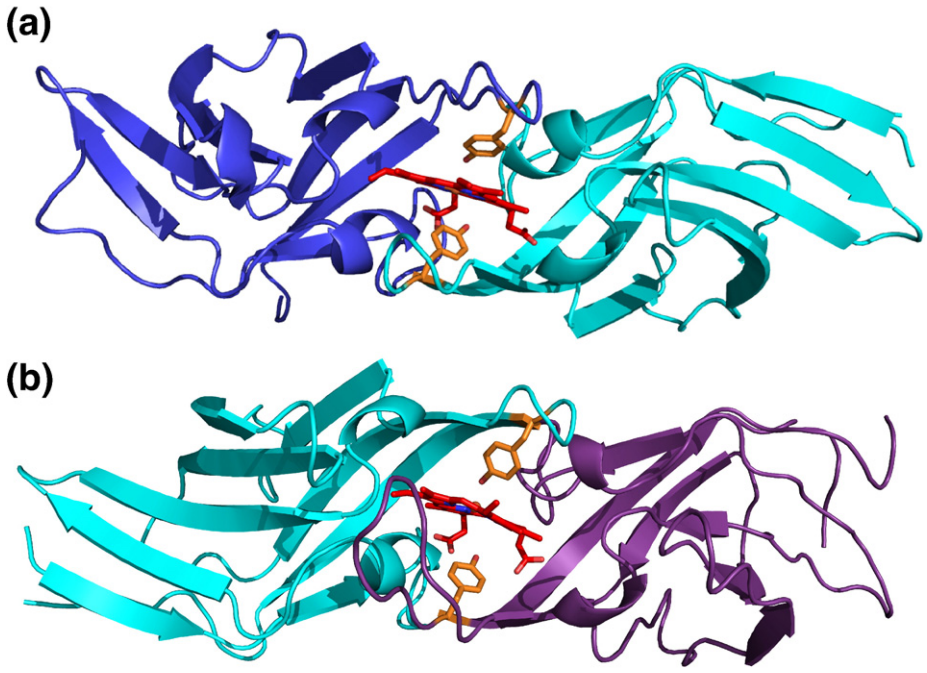

Fig. 7. Model of NEAT domain heme transfer. (a) Model of IsdB-N2-to-IsdA-N1 heme transfer. IsdB-N2 (dark blue) and IsdA-N1 (cyan) are shown as cartoons, with heme and Tyr carbons shown as red and orange sticks, respectively. (b) Model of IsdA-N1-to-IsdC-N1 heme transfer. Shown as in (a), with IsdA-N1 shown in cyan and with IsdC-N1 shown in purple. Models were generated with PyMOL.

access through the sixth coordinate position.[29] Whether heme is directly passed through a stable six-coordinate Tyr_{donor}–Fe(III)–$Tyr_{acceptor}$ intermediate or released by one Tyr and rapidly bound by the other within the confines of a NEAT–NEAT domain complex could not be determined in these experiments, and no absorbance signatures for such an intermediate were detected in multiwavelength stopped-flow experiments.

To date, *S. aureus* Isd protein–protein complexes have eluded unambiguous detection, but it is clear that complexes form in solution because of the rapid rates of heme transfer.[18,34] Rapid heme transfer by means of direct protein–protein interaction has been documented *in vitro* in the related *Bacillus anthracis* heme transport system between two NEAT-domain-containing proteins, BslK and an IsdC homolog.[42,43] Crystal contacts can provide indications of the structure of potential complexes in solution. Although the complexes in crystals are formed between the same protein, these may represent a biologically relevant transfer reaction as well, since heme relay occurs across the ~30-nm cell wall of *S. aureus*[44] and thus may require self-exchange reactions. Generally, the crystal structures of IsdA–heme[29] and its variants from different crystal forms (this work)—IsdB-N2,[30] IsdC heme,[31] and IsdH-N3 heme[32]—display strikingly similar crystal packing interactions. The common motif is two molecules interacting across the heme binding pocket related by an ~180° rotation (Fig. S5). Although two heme groups are present at the interface of the holoproteins, the domains are oriented such that, with a single heme present, a modest conformational change would allow coordination by a sixth heme-iron ligand from the Tyr residue in the neighboring molecule. If a similar complex were to form in solution with heme in only the donor molecule, this model would support heme transfer from Tyr of the donor to Tyr of the receptor, possibly with a bis-Tyr heme intermediate. To examine the potential to form these complexes in solution, we used the protein–protein complex modeling server ClusPro[45,46] to predict unbiased optimal IsdB-N2–IsdA-N1 and IsdA-N1–IsdC-N1 complexes. The heme ligand was not modeled at the interface in ClusPro, but again, the top solutions were strikingly similar to the interactions observed in crystal packing (Fig. S6). The protein–protein complexes, although packed much more closely in the absence of heme, display the same orientations related by a 180° rotation relative to one another such that the heme-iron-coordinating Tyr residues could occupy opposite sides of a heme iron. With crystal packing and ClusPro docking as guide, a model of the proposed heme transfer pair was constructed using PyMOL (Fig. 7).[47]

In the absence of a direct experimental observation of complex formation, our structural, kinetic, and modeling data support the formation of a heme

transfer pair that directs heme iron from the Tyr of the donor to the Tyr of the acceptor. The absence of a detected transient spectroscopic signature for the intermediate can be explained by the high rates of transfer (>10 s^{-1}). Work to stabilize transfer complexes for more detailed characterization and validation of the transfer model is ongoing.

Materials and Methods

Cloning and site-directed mutagenesis

The IsdA-N1 coding region (Ser62-Ala184) was previously cloned into pET28a.[29] Site-directed mutagenesis of pET28a-IsdA-N1 was performed using a modification of the whole plasmid PCR technique described previously.[48] Mutagenic primers are shown in Table S1. IsdB-N2 (residues 341–458) and IsdC-N1 (residues 22–152) were PCR amplified from *S. aureus* N315 genomic DNA and cloned into pET28a to include an N-terminal His_6 tag and a thrombin cleavage site. All genetic manipulations were carried out in *Escherichia coli* DH5α, and mutations were confirmed by DNA sequencing.

Protein expression

His_6-tagged recombinant protein was expressed in *E. coli* BL21(DE3). We inoculated 2× YT media containing 25 μg/ml kanamycin (1:500) from a 5-ml overnight culture in LB containing 25 μg/ml kanamycin. Cultures were incubated at 30 °C, with shaking, for approximately 6 h until an OD_{600} (optical density at 600 nm) of ~0.8 had been reached. Culture temperatures were then shifted to 25 °C, induced with 0.4 mM isopropyl β-D-thiogalactosidase, and incubated for a further 16 h. Cells were lysed using an Emulsi Flex-C5 homogenizer (Avestin, Ottawa, Canada), cell debris was pelleted by centrifugation, and His_6-tagged IsdA-N1 was separated with a HisTrap HP column (GE Healthcare, Piscataway, NJ). His_6-IsdA-N1 was then dialyzed into 50 mM Tris (pH 8.0) and 100 mM NaCl, and His_6-tags were removed by thrombin cleavage. Apo-IsdA-N1 was separated from the partially heme-loaded sample using Source 15S resin (GE Healthcare) after dialysis into 50 mM Hepes (pH 7.2). As required, apoprotein was reconstituted with heme by slow addition of a 1.2× molar excess of heme. Heme stock was freshly prepared by dissolving 2.5 mg of hemin chloride in 100 μl of 0.1 M NaOH and diluting to 1 ml with 50 mM phosphate buffer (pH 7.4). Unbound heme was removed by centrifugation and then passed over a Sephadex G-50 column. Finally, holoprotein was dialyzed into 20 mM Tris (pH 8.0) for crystallization, and apo-IsdA-N1 or holo-IsdA-N1 was dialyzed into 50 mM Tris (pH 8.0) and 100 mM NaCl for all kinetic measurements.

Crystallization

Only wild-type IsdA-N1 produced diffraction-quality crystals on hanging-drop plates with 0.1 M 4-morpholineethanesulfonic acid (pH 6.5), 0.2 M ammonium sulfate, and 30% polyethylene glycol (PEG) 6000, as previously reported.[29] Crystals of IsdA-N1 H83A were obtained under a similar condition with 0.1 M 2-[bis(2-hydroxyethyl)amino]-2-(hydroxymethyl)propane-1,3-diol (pH 5.5), 0.2 M ammonium sulfate, and 25% PEG 3350. Crystals of IsdA-N1 K75A formed in 0.1 M citrate (pH 3.5) with 2–2.2 M ammonium sulfate, and IsdA-N1 Y166A crystals were optimized in 0.1 M Hepes (pH 7.5) and 2.0 M ammonium sulfate. IsdA-N1–CoPPIX crystals were optimized in 0.1 M citrate (pH 3.5) and 1.5 M ammonium sulfate. Crystals under PEG-containing conditions were frozen in mother liquor supplemented with 16% glycerol, whereas crystals under ammonium sulfate conditions supplemented with 30% glycerol were frozen. In both cases, crystals were immersed in cryoprotectant for ~10 s prior to flash freezing in liquid nitrogen. Mother liquor was supplemented with 10 mM dithionite and crystals were soaked for ~10 min prior to flash freezing to attain the IsdA-N1 reduced structure.

Data processing and structure solution

Data were collected on beamline 08ID-1 at the Canadian Light Source (IsdA-N1 reduced, IsdA-N1–CoPPIX, and IsdA-N1 Y166A) and on beamline 7-1 at the Stanford Synchrotron Radiation Lightsource (IsdA-N1 K75A and IsdA-N1 H83A). Data were processed using HKL2000[49] or iMosflm.[50] Phases were determined with the program MOLREP[51] using a single-protein chain of the previously determined IsdA-N1 crystal structure (PDB ID: 2ITF), with heme and water molecules omitted and with several heme binding residues (Lys75, Ser82, His83, Tyr166, and Tyr170) substituted with alanine. Refmac5[52] from the CCP4 program suite[53] and Coot[54] were used to refine and modify the structures. Density for heme (or CoPPIX) was clearly defined in all structures by a prominent metal peak, and heme or CoPPIX was modelled into the binding site prior to water addition. Waters were added with ArpWaters[55] or Coot.[54] Since all unit cells contain multiple molecules, comparative measurements are made using chain A, unless stated otherwise. Data collection and refinement statistics are shown in Table 1. All structure figures were generated using PyMOL.[47]

UV/Visible absorbance spectroscopy

All UV/visible absorbance spectroscopy readings of protein or heme concentrations and heme release experiments were performed using a Cary 50 UV–Vis spectrophotometer (Agilent Technologies, Mississauga, Canada). Heme concentrations were determined using the pyridine hemochrome assay with an extinction coefficient of 191.5 mM^{-1} cm^{-1} at 418 nm.[39]

Determination of heme transfer to myoglobin

Apomyoglobin was prepared from horse heart myoglobin (Sigma), as previously described.[56] Holo-IsdA variants (2 μM) were incubated with 50 μM apomyoglobin, and spectra (250–650 nm) were recorded for 2–30 h, depending on the variant. All transfers were performed at least in duplicate. Absorption differences could be fitted to single-exponential or double-exponential equations using

GraphPad Prism software to determine the first-order rate constants. The concentration of apomyoglobin was varied to ensure that the rate was first order with respect to IsdA-N1.

Kinetics of heme transfer

Absorption spectra (300–700 nm) were collected using an SX.18MV stopped-flow reaction analyzer (Applied Photophysics, Leatherhead, UK) equipped with a photodiode array detector. All experiments were performed at 25 °C. To determine the wavelength of maximal absorbance change, we mixed 2 μM holoprotein with 20 μM apoprotein, and we calculated the difference spectra between the initial reading and 100 subsequent time points logarithmically distributed over 10 s. For most reactions, absorbance changed maximally at ~376 nm. For calculation of the observed rate (k_{obs}), the SX.18MV monochrometer was used to monitor absorbance at 376 nm. For all transfer pairs, 1 μM holo-IsdA-N1 or 4 μM holo-IsdB-N2 was mixed with 10–100 μM apo-IsdC-N1 or apo-IsdA-N1, respectively. Single-wavelength data were collected for >10 half-lives (between 0.1 s and 5 s, depending on the variant). Values for k_{obs} were obtained from at least five independent reactions. Change in absorbance data was fitted to single-exponential equations using GraphPad Prism software. Observed transfer rates were plotted against the concentration of apoprotein to determine the concentration dependence and transfer rates.

Accession numbers

PDB coordinates have been deposited in the Research Collaboratory for Structural Bioinformatics PDB under accession numbers 3QZN (IsdA-N1 Y166A), 3QZM (IsdA-N1 H83A), 3QZL (IsdA-N1 K75A), 3QZP (IsdA-N1–CoPPIX), and 3QZO (IsdA-N1 reduced).

Supplementary materials related to this article can be found online at doi:10.1016/j.jmb.2011.08.047

Acknowledgements

This work was supported by a Canadian Institutes of Health Research operating grant (MOP-49597) to M.E.P.M. J.C.G. was supported by a Natural Sciences and Engineering Research Council of Canada CGS Doctoral Award and a Michael Smith Foundation for Health Research Junior Graduate Trainee Award.

Portions of the research described in this article were performed at the Canadian Light Source (supported by the Natural Sciences and Engineering Research Council of Canada, the National Research Council Canada, the Canadian Institutes of Health Research, and the University of Saskatchewan) and at the Stanford Synchrotron Radiation Light Source (a national user facility operated by Stanford University on behalf of the US Department of Energy, Office of Basic Energy Sciences). The SSRL Structural Molecular Biology Program was supported by the Department of Energy Office of Biological and Environmental Research and by the National Institutes of Health National Center for Research Resources, Biomedical Technology Program, and the National Institute of General Medical Sciences.

We would like to thank Angele Arrieta for technical assistance, and Dr. Lindsay Eltis, Dr. Rahul Singh, Dr. Federico Rosell, and Anthony Ruzzini for helpful discussion and assistance with the stopped-flow kinetics. We would also like to thank Catherine Gaudin and Anson Chan for critical reading of the manuscript.

References

1. Wandersman, C. & Delepelaire, P. (2004). Bacterial iron sources: from siderophores to hemophores. *Annu. Rev. Microbiol.* **58**, 611–647.
2. Radtke, A. L. & O'Riordan, M. X. (2006). Intracellular innate resistance to bacterial pathogens. *Cell. Microbiol.* **8**, 1720–1729.
3. Ratledge, C. & Dover, L. G. (2000). Iron metabolism in pathogenic bacteria. *Annu. Rev. Microbiol.* **54**, 881–941.
4. Stojiljkovic, I. & Perkins-Balding, D. (2002). Processing of heme and heme-containing proteins by bacteria. *DNA Cell Biol.* **21**, 281–295.
5. Klevens, R. M., Morrison, M. A., Nadle, J., Petit, S., Gershman, K., Ray, S. *et al.* (2007). Invasive methicillin-resistant *Staphylococcus aureus* infections in the United States. *J. Am. Med. Assoc.* **298**, 1763–1771.
6. Lowy, F. D. (1998). *Staphylococcus aureus* infections. *N. Engl. J. Med.* **339**, 520–532.
7. Klevens, R. M., Edwards, J. R., Tenover, F. C., McDonald, L. C., Horan, T. & Gaynes, R. (2006). Changes in the epidemiology of methicillin-resistant *Staphylococcus aureus* in intensive care units in US hospitals, 1992–2003. *Clin. Infect. Dis.* **42**, 389–391.
8. Beasley, F. C., Vines, E. D., Grigg, J. C., Zheng, Q., Liu, S., Lajoie, G. A. *et al.* (2009). Characterization of staphyloferrin A biosynthetic and transport mutants in *Staphylococcus aureus*. *Mol. Microbiol.* **72**, 947–963.
9. Cotton, J. L., Tao, J. & Balibar, C. J. (2009). Identification and characterization of the *Staphylococcus aureus* gene cluster coding for staphyloferrin A. *Biochemistry*, **48**, 1025–1035.
10. Cheung, J., Beasley, F. C., Liu, S., Lajoie, G. A. & Heinrichs, D. E. (2009). Molecular characterization of staphyloferrin B biosynthesis in *Staphylococcus aureus*. *Mol. Microbiol.* **74**, 594–608.
11. Sebulsky, M. T. & Heinrichs, D. E. (2001). Identification and characterization of fhuD1 and fhuD2, two genes involved in iron–hydroxamate uptake in *Staphylococcus aureus*. *J. Bacteriol.* **183**, 4994–5000.
12. Dale, S. E., Sebulsky, M. T. & Heinrichs, D. E. (2004). Involvement of SirABC in iron–siderophore import in *Staphylococcus aureus*. *J. Bacteriol.* **186**, 8356–8362.
13. Sebulsky, M. T., Hohnstein, D., Hunter, M. D. & Heinrichs, D. E. (2000). Identification and characterization of a membrane permease involved in iron–

hydroxamate transport in *Staphylococcus aureus*. *J. Bacteriol.* **182**, 4394–4400.
14. Mazmanian, S. K., Skaar, E. P., Gaspar, A. H., Humayun, M., Gornicki, P., Jelenska, J. *et al.* (2003). Passage of heme-iron across the envelope of *Staphylococcus aureus*. *Science*, **299**, 906–909.
15. Skaar, E. P., Humayun, M., Bae, T., DeBord, K. L. & Schneewind, O. (2004). Iron-source preference of *Staphylococcus aureus* infections. *Science*, **305**, 1626–1628.
16. Skaar, E. P. & Schneewind, O. (2004). Iron-regulated surface determinants (Isd) of *Staphylococcus aureus*: stealing iron from heme. *Microbes Infect.* **6**, 390–397.
17. Grigg, J. C., Ukpabi, G., Gaudin, C. F. & Murphy, M. E. (2010). Structural biology of heme binding in the *Staphylococcus aureus* Isd system. *J. Inorg. Biochem.* **104**, 341–348.
18. Zhu, H., Xie, G., Liu, M., Olson, J. S., Fabian, M., Dooley, D. M. & Lei, B. (2008). Pathway for heme uptake from human methemoglobin by the iron-regulated surface determinants system of *Staphylococcus aureus*. *J. Biol. Chem.* **283**, 18450–18460.
19. Speziali, C. D., Dale, S. E., Henderson, J. A., Vines, E. D. & Heinrichs, D. E. (2006). Requirement of *Staphylococcus aureus* ATP-binding cassette–ATPase FhuC for iron-restricted growth and evidence that it functions with more than one iron transporter. *J. Bacteriol.* **188**, 2048–2055.
20. Grigg, J. C., Vermeiren, C. L., Heinrichs, D. E. & Murphy, M. E. (2007). Heme coordination by *Staphylococcus aureus* IsdE. *J. Biol. Chem.* **282**, 28815–28822.
21. Lee, W. C., Reniere, M. L., Skaar, E. P. & Murphy, M. E. P. (2008). Ruffling of metalloporphyrins bound to IsdG and IsdI, two heme-degrading enzymes in *Staphylococcus aureus*. *J. Biol. Chem.* **283**, 30957–30963.
22. Skaar, E. P., Gaspar, A. H. & Schneewind, O. (2004). IsdG and IsdI, heme-degrading enzymes in the cytoplasm of *Staphylococcus aureus*. *J. Biol. Chem.* **279**, 436–443.
23. Reniere, M. L., Ukpabi, G. N., Harry, S. R., Stec, D. F., Krull, R., Wright, D. W. *et al.* (2010). The IsdG-family of haem oxygenases degrades haem to a novel chromophore. *Mol. Microbiol.* **75**, 1529–1538.
24. Andrade, M. A., Ciccarelli, F. D., Perez-Iratxeta, C. & Bork, P. (2002). NEAT: a domain duplicated in genes near the components of a putative Fe^{3+} siderophore transporter from Gram-positive pathogenic bacteria. *Genome Biol.* **3**; RESEARCH0047.1-0047.5.
25. Pluym, M., Muryoi, N., Heinrichs, D. E. & Stillman, M. J. (2008). Heme binding in the NEAT domains of IsdA and IsdC of *Staphylococcus aureus*. *J. Inorg. Biochem.* **102**, 480–488.
26. Tiedemann, M. T., Muryoi, N., Heinrichs, D. E. & Stillman, M. J. (2008). Iron acquisition by the haem-binding Isd proteins in *Staphylococcus aureus*: studies of the mechanism using magnetic circular dichroism. *Biochem. Soc. Trans.* **36**, 1138–1143.
27. Vermeiren, C. L., Pluym, M., Mack, J., Heinrichs, D. E. & Stillman, M. J. (2006). Characterization of the heme binding properties of *Staphylococcus aureus* IsdA. *Biochemistry*, **45**, 12867–12875.
28. Tiedemann, M. T., Muryoi, N., Heinrichs, D. E. & Stillman, M. J. (2009). Characterization of IsdH (NEAT domain 3) and IsdB (NEAT domain 2) in *Staphylococcus aureus* by magnetic circular dichroism spectroscopy and electrospray ionization mass spectrometry. *J. Porphyrins Phthalocyanines*, **13**, 1006–1016.
29. Grigg, J. C., Vermeiren, C. L., Heinrichs, D. E. & Murphy, M. E. P. (2007). Haem recognition by a *Staphylococcus aureus* NEAT domain. *Mol. Microbiol.* **63**, 139–149.
30. Gaudin, C. F., Grigg, J. C., Arrieta, A. L. & Murphy, M. E. (2011). Unique heme-iron coordination by the hemoglobin receptor IsdB of *Staphylococcus aureus*. *Biochemistry*, **50**, 5443–5452.
31. Sharp, K. H., Schneider, S., Cockayne, A. & Paoli, M. (2007). Crystal structure of the heme–IsdC complex, the central conduit of the Isd iron/heme uptake system in *Staphylococcus aureus*. *J. Biol. Chem.* **282**, 10625–10631.
32. Watanabe, M., Tanaka, Y., Suenaga, A., Kuroda, M., Yao, M., Watanabe, N. *et al.* (2008). Structural basis for multimeric heme complexation through a specific protein–heme interaction: the case of the third neat domain of IsdH from *Staphylococcus aureus*. *J. Biol. Chem.* **283**, 28649–28659.
33. Villareal, V. A., Pilpa, R. M., Robson, S. A., Fadeev, E. A. & Clubb, R. T. (2008). The IsdC protein from *Staphylococcus aureus* uses a flexible binding pocket to capture heme. *J. Biol. Chem.* **283**, 31591–31600.
34. Liu, M., Tanaka, W. N., Zhu, H., Xie, G., Dooley, D. M. & Lei, B. (2008). Direct hemin transfer from IsdA to IsdC in the iron-regulated surface determinant (Isd) heme acquisition system of *Staphylococcus aureus*. *J. Biol. Chem.* **283**, 6668–6676.
35. Muryoi, N., Tiedemann, M. T., Pluym, M., Cheung, J., Heinrichs, D. E. & Stillman, M. J. (2008). Demonstration of the iron-regulated surface determinant (Isd) heme transfer pathway in *Staphylococcus aureus*. *J. Biol. Chem.* **283**, 28125–28136.
36. Laskowski, R. A., MacArthur, M. W., Moss, D. S. & Thornton, J. M. (1993). PROCHECK: a program to check the stereochemical quality of protein structures. *J. Appl. Crystallogr.* **26**, 283–291.
37. Eakanunkul, S., Lukat-Rodgers, G. S., Sumithran, S., Ghosh, A., Rodgers, K. R., Dawson, J. H. & Wilks, A. (2005). Characterization of the periplasmic heme-binding protein shut from the heme uptake system of *Shigella dysenteriae*. *Biochemistry*, **44**, 13179–13191.
38. Torres, V. J., Pishchany, G., Humayun, M., Schneewind, O. & Skaar, E. P. (2006). *Staphylococcus aureus* IsdB is a hemoglobin receptor required for heme iron utilization. *J. Bacteriol.* **188**, 8421–8429.
39. Fuhrhop, J. H. & Smith, K. M. (1975). Laboratory methods. In *Porphyrins and Metalloporphyrins* (Smith, K. M., ed.), pp. 804–807, Elsevier Publishing Co., New York, NY.
40. Clarke, S. R., Brummell, K. J., Horsburgh, M. J., McDowell, P. W., Mohamad, S. A., Stapleton, M. R. *et al.* (2006). Identification of *in vivo*-expressed antigens of *Staphylococcus aureus* and their use in vaccinations for protection against nasal carriage. *J. Infect. Dis.* **193**, 1098–1108.
41. Ran, Y., Zhu, H., Liu, M., Fabian, M., Olson, J. S., Aranda, R., IV *et al.* (2007). Bis-methionine ligation to heme iron in the streptococcal cell surface protein Shp facilitates rapid hemin transfer to HtsA of the HtsABC transporter. *J. Biol. Chem.* **282**, 31380–31388.

42. Tarlovsky, Y., Fabian, M., Solomaha, E., Honsa, E., Olson, J. S. & Maresso, A. W. (2010). A *Bacillus anthracis* S-layer homology protein that binds heme and mediates heme delivery to IsdC. *J. Bacteriol.* **192**, 3503–3511.
43. Fabian, M., Solomaha, E., Olson, J. S. & Maresso, A. W. (2009). Heme transfer to the bacterial cell envelope occurs via a secreted hemophore in the Gram-positive pathogen *Bacillus anthracis*. *J. Biol. Chem.* **284**, 32138–32146.
44. Beveridge, T. J. & Matias, V. R. (2006). Ultrastructure of Gram-positive cell walls. In *Gram-Positive Pathogens* (Fischetti, V. A., Novick, R. P., Ferretti, J. J., Portnoy, D. A. & Rood, J. I., eds), pp. 3–11, 2nd edit. ASM Press, Washington, DC.
45. Comeau, S. R., Kozakov, D., Brenke, R., Shen, Y., Beglov, D. & Vajda, S. (2007). ClusPro: performance in CAPRI rounds 6–11 and the new server. *Proteins*, **69**, 781–785.
46. Comeau, S. R., Gatchell, D. W., Vajda, S. & Camacho, C. J. (2004). ClusPro: a fully automated algorithm for protein–protein docking. *Nucleic Acids Res.* **32**, W96–W99.
47. DeLano, W. L. (2008). *The PyMOL Molecular Graphics System.* DeLano Scientific LLC, Palo Alto, CA.
48. MacPherson, I. S., Rosell, F. I., Scofield, M., Mauk, A. G. & Murphy, M. E. (2010). Directed evolution of copper nitrite reductase to a chromogenic reductant. *Protein Eng. Des. Sel.* **23**, 137–145.
49. Otwinowski, Z. & Minor, W. (1997). Processing of X-ray diffraction data collected in oscillation mode. *Methods Enzymol.* **276**, 307–326.
50. Leslie, A. G. W. (1992). Recent changes to the MOSFLM package for processing film and image plate data. *Jt. CCP4 ESF-EACMB Newsl. Protein Crystallogr.* **26**, 27–33.
51. Vagin, A. & Teplyakov, A. (1997). MOLREP: an automated program for molecular replacement. *J. Appl. Crystallogr.* **30**, 1022–1025.
52. Murshudov, G. N., Vagin, A. A. & Dodson, E. J. (1997). Refinement of macromolecular structures by the maximum-likelihood method. *Acta Crystallogr., Sect. D: Biol. Crystallogr.* **53**, 240–255.
53. CCP4 (1994). The CCP4 suite: programs for protein crystallography. *Acta Crystallogr., Sect. D: Biol. Crystallogr.* **50**, 760–763.
54. Emsley, P. & Cowtan, K. (2004). Coot: model-building tools for molecular graphics. *Acta Crystallogr., Sect. D: Biol. Crystallogr.* **60**, 2126–2132.
55. Lamzin, V. S. & Wilson, K. S. (1997). Automated refinement for protein crystallography. *Methods Enzymol.* **277**, 269–305.
56. Teale, F. W. (1959). Cleavage of the haem–protein link by acid methylethylketone. *Biochim. Biophys. Acta*, **35**, 543.